ORIGINAL PAPER

CrossMark

Rotating-disk electrospinning: needleless electrospinning of poly(caprolactone), poly(lactic acid) and poly(vinyl alcohol) nanofiber mats with controlled morphology

Jun-Jye Ng [1] · Pitt Supaphol [1,2]

Abstract

As a contribution to the feasibility of high-throughput electrospinning, here we report on the investigation into the production of polymer nanofiber mats through needleless electrospinning. For this study, we used poly(caprolactone) (PCL), poly(lactic acid) (PLA) and poly(vinyl alcohol) (PVA), widely used polymers in the field of electrospinning. Optimization studies were carried out to devise the characteristics of the rotating-disk electrospinning system in order to assess the processing window for each polymer. Other factors were also considered, where the production rate, fiber size distribution, and morphology of the specimens acquired by rotating-disk electrospinning and conventional electrospinning techniques were compared. Our studies also illustrate the similarities of this novel "bottom-up" process compared to the conventional one, where a high resolution image confirmed the formation of a cone-jet structure and a Taylor Cone.

Keywords Electrospinning · Mass production · High throughput · Nanofiber · Needleless electrospinning

Introduction

Polymeric nanofibers can be processed by phase separation [1], template synthesis [2, 3], filament drawing, self-assembly [4], fibrillation [5], island-in-sea [6], nano-lithography [7], and electrospinning. Out of the mentioned methods, electrospinning has the highest potential for industrial application due to its high repeatability and good control on fiber dimensions. Electrospinning is an exceptionally simple method to produce non-woven nanofibers from both synthetic and natural polymers, and the vast range of applications of electrospun nanofiber mats include the biomedical fields [8] such as drug delivery [9, 10], tissue engineering [10], and wound dressing [11] and there is also an important role to play in the filtration industry [12, 13], sensors, electronics [3] and so forth [14].

The conventional electrospinning process, sometimes called single nozzle electrospinning, consists of a high voltage power supply, rotating drum, syringe, needle, and a syringe pump. Although it is a simple technique, the low productivity of conventional single nozzle electrospinning is limiting the industrialization of this method [15, 16]. Recent works have been published that propose feasible up-scaling of electrospinning for industrial application and could be generalized into multi-needle electrospinning and needleless electrospinning [16, 17]. Multi-needle/nozzle arrangements [18–24] are considered to be the most practical and feasible but are more complicated than the conventional single-needle set-up. Studies have gone into investigating the effect of needle number, needle configuration, and needle spacing on the productivity of each set-up. Due to the complexity [25] of up-scaling the multi-needle electrospinning set-up, efforts have been made to develop needleless electrospinning processes that simultaneously eject multiple polymeric jets from the surfaces of polymer solutions. Nonetheless, no matter what method each design uses, electrostatic forces have to overcome any opposing forces acting on the polymer in order to produce polymer jets. Simply put, the system has to reach a threshold voltage [26] for it to create an electric field strength that favors cone-jet formation.

✉ Pitt Supaphol
pitt.s@chula.ac.th

1   The Petroleum and Petrochemical College, Chulalongkorn University, Bangkok 10330, Thailand

2   The Center for Petroleum, Petrochemicals and Advanced Materials, Chulalongkorn University, Bangkok 10330, Thailand

Past studies had explored applications of magnetic fluid [27], ball [28], rotating drum (Nanospider) [29], disk [28, 30], beaded chain [31], spiral coil [31, 32], wire [33, 34], cleft, porous materials [35–37], and bubbles [38–40] as electrospinning nozzles with the objective to improve on the productivity of electrospinning. All of the works mentioned above had a similar concept where the main purpose was to create a surface of the polymeric solution that is thin enough for electrostatic repulsion to occur. Nonetheless, the electric field strength needs to be strong enough to generate polymer jetting and that is why we normally observe polymer jetting at the edges of any large-surfaced electrodes such as a drum or a cleft, where the electric field strength is strongest. Finite element analysis also shows that the electric field strengths on a rotating drum or a disk are the highest at the edges, therefore polymer jets are only observed at these points [30]. Therefore, using a thin disk as an electrode seems to be a promising direction to go as there will be no energy wasted for a large-surfaced electrode like a drum or cleft. In the results reported by Xungai Wang et al. [30], they used a single disk of 2 mm thickness as the nozzle and they successfully produced PVA nanofibers which they explored in terms of the effect of electric field strength on the fiber diameter distribution. However, the threshold voltage of their electrospinning system started at 42 kV which is almost twice the value of the spinning voltage of PVA solution using conventional single nozzle electrospinning.

The main purpose of this study is to investigate whether reducing the thickness of the disk to 1 mm will have an effect on the electric field strength of the system, thus lowering the threshold voltage of electrospinning PVA fibers. Nonetheless, the production rate would also decrease with increasing the nozzle-to-collector gap, and therefore an optimal condition should be identified. As this work aims to promote the mass production of electrospinning, conditions that promote the highest production rate or productivity are further investigated by comparing to samples obtained by conventional electrospinning methods. To further understand the system, organic solvent system polymeric solutions were also investigated to see how the system would behave with different solvent systems.

Experiment

Materials

The series of materials used to fabricate the electrospun nanofiber mats in this study were poly(lactic acid) (PLA; Mn = 200,000 g•mol-1), poly(caprolactone) (PCL; Mn = 80,000 g•mol-1; Aldrich, Madison, WI), poly(vinyl alcohol) (PVA; Mn = 150,000 g•mol-1; Carlo Erba, Rodano, Italy), N,N-dimethylformamide (DMF; LAB-scan Asia, Bangkok,

Thailand), dichloromethane (DCM; Carlo Erba, Rodano, Italy). All materials were of analytical reagent grade and used as received without further purification.

Preparation of polymeric solution

PLA solution was prepared by stirring 10% w/v of PLA in 3:7 v/v DMF/DCM mixed solvent with a magnetic stirrer for 4 h at room temperature. The PCL solution was prepared in a 1:1 v/v mixed solvent of DMF/DCM. The PCL mixture was stirred with a magnetic stirrer for 4 h and the concentration of the PCL solution was 12% w/v. PVA aqueous solution was prepared by stirring 12% w/v PVA powder in distilled water at 90 °C for 5 h, using a silicon oil bath for heating and magnetic stirrer for stirring.

Fabrication of electrospun nanofiber mats

Rotating-disk electrospinning

The prepared polymeric solutions were introduced to the experimental set-up illustrated in Fig. 1 which consists of a 120 mm diameter rotating disk 1 mm thick connected to a motor stand, connected to a DC motor controlling unit, a solution reservoir, an adjustable raiser, a high voltage DC power supply, and three independent collectors. The solution reservoir was placed on the adjustable raiser and filled with polymeric solution. The height of the reservoir was set by adjusting the raiser until the disk was just touching the surface of the solution. The DC motor control unit was turned on and the rotating speed of the disk was set to 30 rpm so that a thin layer of polymer solution was picked up on the edge face of the disk. The high voltage supply was connected directly to the rotating disk by a thin wire electrode briefly touching the side face of the disk. Depending on the polymer solution, the
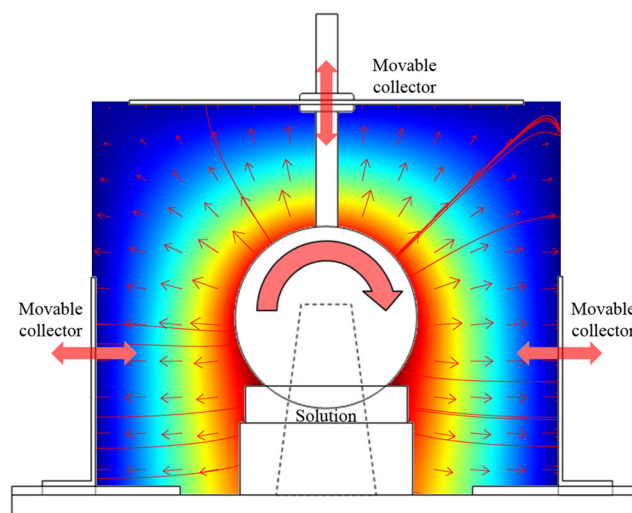

Fig. 1 Schematic illustrating the Rotating-disk electrospinning setup

supplied high DC voltage was set to 24 kV, 25 kV and 28 kV for PLA, PCL and PVA solutions respectively. In this work, the collector-to-disk distance of rotating-disk electrospinning was varied between 8 to 14 cm for all polymer solutions. The collectors were made from acrylic resin, measuring 20 cm wide by 28 cm long, and were placed perpendicular above and both sides to the disk. Aluminum foil was wrapped on the collecting sides of the collectors. When electrical potential was applied, small droplets of polymer solution were formed on the thin layer of polymer solution, forming a cone-jet, and polymeric jets could be observed at the tip of each droplet when the applied voltage exceeded the threshold voltage. Polymer jets were deposited on the earthed collectors where nanofiber mats were formed. The average temperature was 22 °C and relative humidity was 79%.

Conventional electrospinning method

The experimental set-up consisted of an 18-gauge needle attached to the tip of a syringe, a syringe pump, a rotating drum collector, and a high voltage DC power supply. The syringe was held at a 45° angle above the collector as shown in Fig. 2(a). Polymer solution was poured into the syringe and connected to the syringe pump through a tube and rubber bung. High voltage was supplied by attaching a crocodile clip to the needle tip. The collector was wrapped with a layer of aluminum foil and earthed, so that a potential difference that drives the electrospinning process could be created between the needle tip and the collector. The syringe pump was set at 3 ml/h, where it was sufficient to maintain a droplet at the needle tip. The collector-to-needle distance was varied between 10 to 18 cm and the electrospinning voltage was varied between 15 to 21 kV depending on the polymer. The average temperature was 22 °C and relative humidity was 79%.

Characterization

Productivity

To better understand the feasibility of this design, the production rates or the productivity of both electrospinning systems were compared. Nonetheless, the total mass transfer within a given time frame can be calculated as production rate or productivity. The initial weight of the collector was determined and noted along with the final weight of the collector, and the collected fibers were also weighed as a unit and noted after electrospinning. The initial weight was deducted from the final weight to yield the actual spun weight of the collected fiber. This value was then divided by the amount of time used to spin the fibers that was timed using a stopwatch. All results were triplicated.

SEM

Scanning Electron Microscopy (SEM) images were captured by JEOL JSM-5200 scanning electron microscope with a magnification of 5000 times for PLA and PCL and 15,000 times for PVA. Prior to SEM observation, the samples were coated with gold using a JEOL JFC-1100E sputtering device.

Fiber size distribution

Multiple measurements of fiber diameters were made using Semafore software. Pictures taken from SEM were used for sampling. For each condition, three pictures were chosen from a series of SEM images. Since all conditions were triplicated, one picture from each repetition was chosen and measurements were made on fibers at the foreground. A tally was made for different diameter ranges with 100 nm increments for each range. Two hundred measurement points were made for each condition.

Taylor cone analysis

Photographs of the electrospinning process were taken by a high resolution digital single reflex camera (DSLR camera) and later cropped to show only a single droplet of polymeric solution. The image was then adjusted in Adobe Photoshop CS3 to monochrome in order to show the details of the Taylor Cone and the spinning jet clearer. The image was then used to measure the Taylor Cone angle using Semafore software.

Results and discussion

Rotating-disk electrospinning

An initial study was carried out to identify the favorable electrospinning window for each polymer. It was clearly obvious at the initial stage of the experiment that the critical or threshold voltages of the conventional single nozzle electrospinning for all three polymers were not enough, as hypothesized, as we were now working against gravity; there were more forces to overcome. Even at the shortest distance of 8 cm, where the electric field strength is strongest, no jetting was observed at the same electrospinning voltage (20 kV, 21 kV, and 15 kV for 10% PLA, 12% PCL, and 12% PVA respectively) matching the conventional electrospinning method. However, jetting of the polymer solution started at slightly higher voltages of 24 kV, 25 kV, and 28 kV for 10% PLA, 12% PCL, and 12% PVA respectively, and jetting continuously occurred for the entire range of disk to collector distances starting from 8 cm up to 14 cm. On the other hand, the cone-jet did not
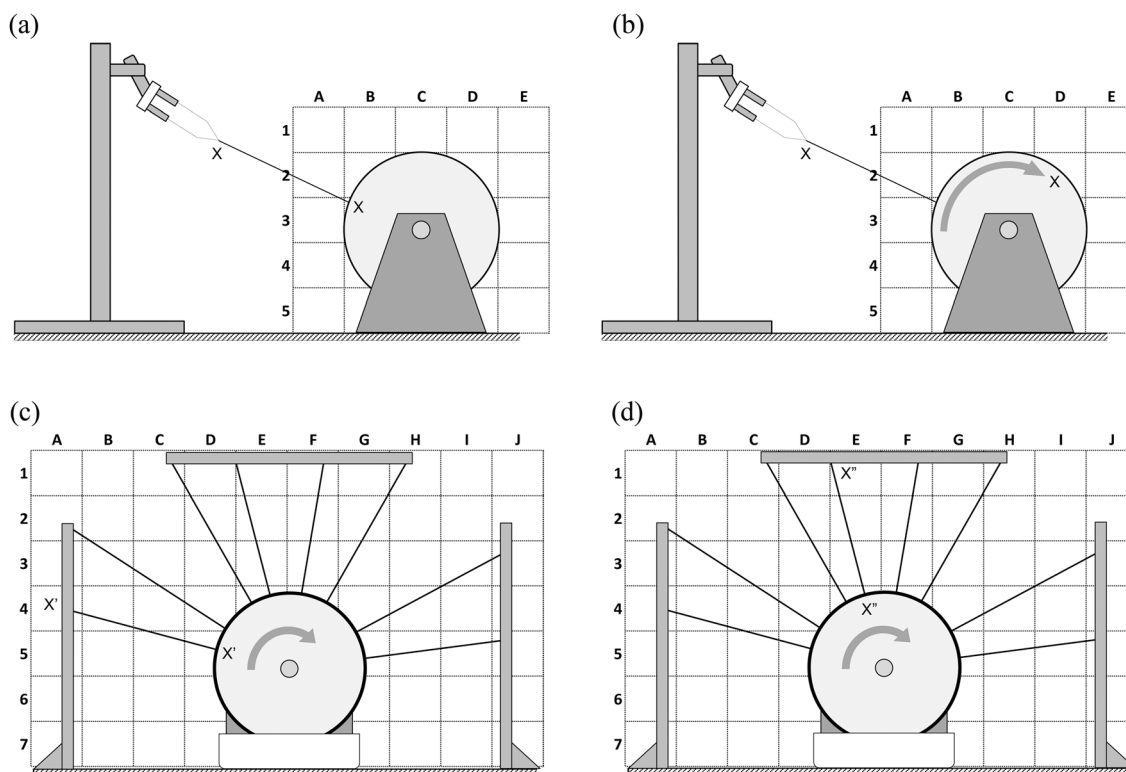
Fig. 2 Comparison between (**a**) Conventional electrospinning technique at time = t_0, (**b**) Conventional electrospinning technique at any time of time = t_1, (**c**) Rotating-disk electrospinning technique at time = t_0, (**d**) Rotating-disk electrospinning technique at any time of time = t_1

occur at the edge of the disk instantaneously after the disk had left the solution bath at the reservoir due to surface tension of the polymer layer.

As the disk rotated further, the solution layer flowed backwards due to gravitational pull, thus causing a thinner layer. As the layer got thinner, the surface tension created on the polymer surface reduced to a point where electrostatic forces exceeded all opposing forces and a cone-jet structure was formed [26, 41], as shown in Fig. 3 and Fig. 4. To further establish an understanding of its effects on the electrospinning of polymers, the rotational speed of the rotating disk was varied. At a lower rotational speed, the polymer layer that was formed on the edge face of the disk developed into a thinner, more spin-able thickness (as described above) much sooner. As a result, we could observe that the cone-jet was seen forming sooner (closer to the reservoir). However, if the rotational speed is too slow, the polymer layer will dry up as it has more time to interact with the air. On the other hand, if we increase the rotational speed, the cone-jet can be seen forming "late", which means the polymer layer did not have enough time to flow and reach a favorable condition (in this case, the thickness of the polymer layer) but the polymer layer managed to maintain its viscosity as there was not enough time for the solvent to evaporate. By observing these positive and negative effects, the best condition would be at a rotational speed of 30 rpm, where uniform formations of multiple cone-jets were observed.

All three polymers gave the same outcome where only vigorous jetting and spurting occurred at distances between 8 cm to 10 cm as a result of the strong electric field. This resulted in a layer of wet polymer solution laid over the collectors due to insufficient time for the solvent to evaporate. This resulted in a polymer film when left to dry, and these conditions would be more suitable to be called "mass transfer" rather than electrospinning. However, as the distance was increased further than 10 cm, the electric field became more favorable towards electrospinning.
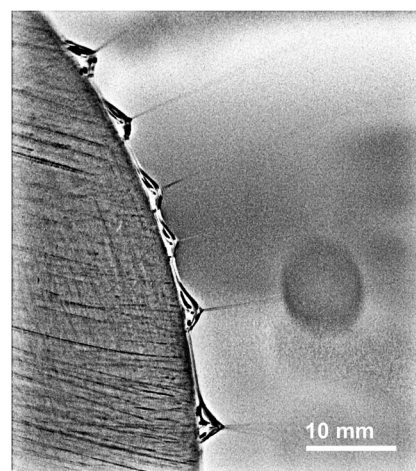

Fig. 3 Image of multiple cone-jets forming on the edge face of the disk nozzle
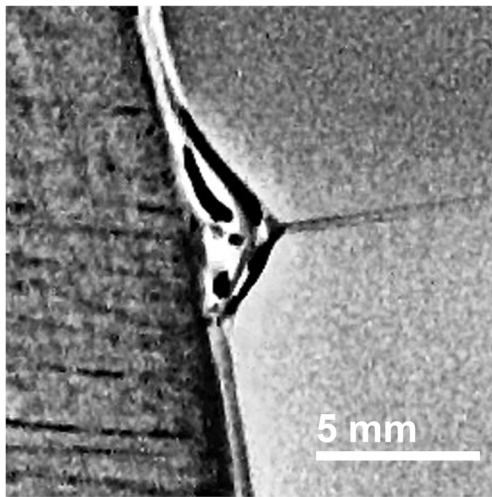
Fig. 4 Close up image on a cone-jet forming on a single polymer droplet that was formed on the edge face of the spinning disk. A layer of polymer solution and a cone-jet is shown in this image

In conventional single nozzle electrospinning, it could be described as a single-point-to-single-point system where a single cone-jet is formed and collected at a single "random" point on the collector. Since the polymer jet is whipping at the end of the straight polymer jet, which is called bending instability, a network of nanofiber mats is formed on both a stationary or rotating collector. In the rotating-disk electrospinning system, the disk is rotating continuously and the starting point of the polymer jet remains the same, but the reference deposition point is relocated at a new point.

As seen in the schematic in Fig. 2(a) and (b), the nozzle initially spins from the needle tip to point X. As the rotating drum is rotated to a new position, the original point X is in another position while the polymer jet still retains its original geometry (starting at the needle tip and ending at the drum at position B-3 on the grid). The polymer jet will always start at the same point and ends up at the same point hypothetically
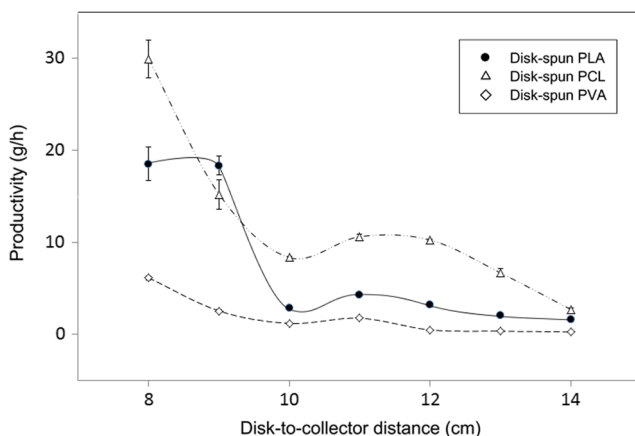
Fig. 5 Productivity (g/h) in relation to disk-to-collector distances for 10% w/v PLA in 3:7 v/v DMF/DCM, 12% w/v PCL in 1:1 v/v DMF/DCM and 12% w/v PVA aqueous solution

(although there is a whipping action), and a mat is formed as the collecting drum rotates. As for the rotating-disk electrospinning shown in Fig. 2(c), the first jet can be seen forming at around 20° starting at the polymer solution layer at point X' situated at position D-5 and ending on the collector at position A-4. As the disk rotates further (as shown in Fig. 2(d)), the exact cone-jet originally at X' has repositioned at point X" at position E-4 on the disk, ending up at position E-1 on the top collector. We have called this a multiple-point-to-multiple-point system.

Productivity

All polymer solutions showed similar trends in productivity figures. The production rate would be the highest at greater distance and decreases as the disk-to-collector distance increases; but will reach the lowest value at around 10 cm. From observation, there were only instances of vigorous jetting and spurting of polymer solutions from the disk to collector as the distance of less than 10 cm created a strong electric field that promotes only jetting and spurting. Moreover, there was not enough time for the solvents to evaporate at disk-to-collector distances of less than 10 cm so only polymer films were deposited at the collector. In the study, the system was most stable for all polymeric systems between 11 cm and 12 cm where the productivity is highest and uniform jetting of polymer solutions was observed. This leads to a uniform deposition of polymeric nanofibers at the collector where SEM images showed that all individual fibers are uniform and well distributed. Therefore, we can say that there are two regions: the unstable region and the stable region.

Conditions with disk-to-collector distance of 11 cm were chosen and studied further because all polymers spun stably and yielded the highest productivity as presented in Fig. 5. At 11 cm, it is the beginning of the stable region and the productivity was highest but then declined as the disk-to-collector distance was increased. This is expected as the electric field strength would decrease with increasing distance. The production rate for 10% w/v PLA, 12% w/v PCL, and 12% w/v PVA was 4.254 ± 0.150 g/h, 10.611 ± 0.233 g/h and 1.721 ± 0.116 g/h respectively. The production rates for conventional single nozzle setup were also investigated and were 0.312 ± 0.150 g/h, 0.128 ± 0.233 g/h, and 0.027 ± 0.116 g/h respectively. The initial purpose of disk electrospinning was to introduce multiple droplets on the spinneret (disk) so that it could mimic multi-nozzle systems proposed by researchers such as Ying Yang et al. and the authors of similar studies.

SEM images

Continuous formation of polymer nanofiber could be observed and no beaded-fibers were present, which meant that favorable conditions were achieved. The morphologies of the

Table 1 SEM images of (a) PLA nanofibers from conventional electrospinning, (b) from Rotating-disk electrospinning, (c) PCL nanofibers from conventional electrospinning, (d) from Rotating-disk electrospinning, (e) PVA nanofibers from conventional electrospinning and (f) from Rotating-disk electrospinning. The magnification for the PLA and PCL images is 5000 times and 15,000 times for PVA images.
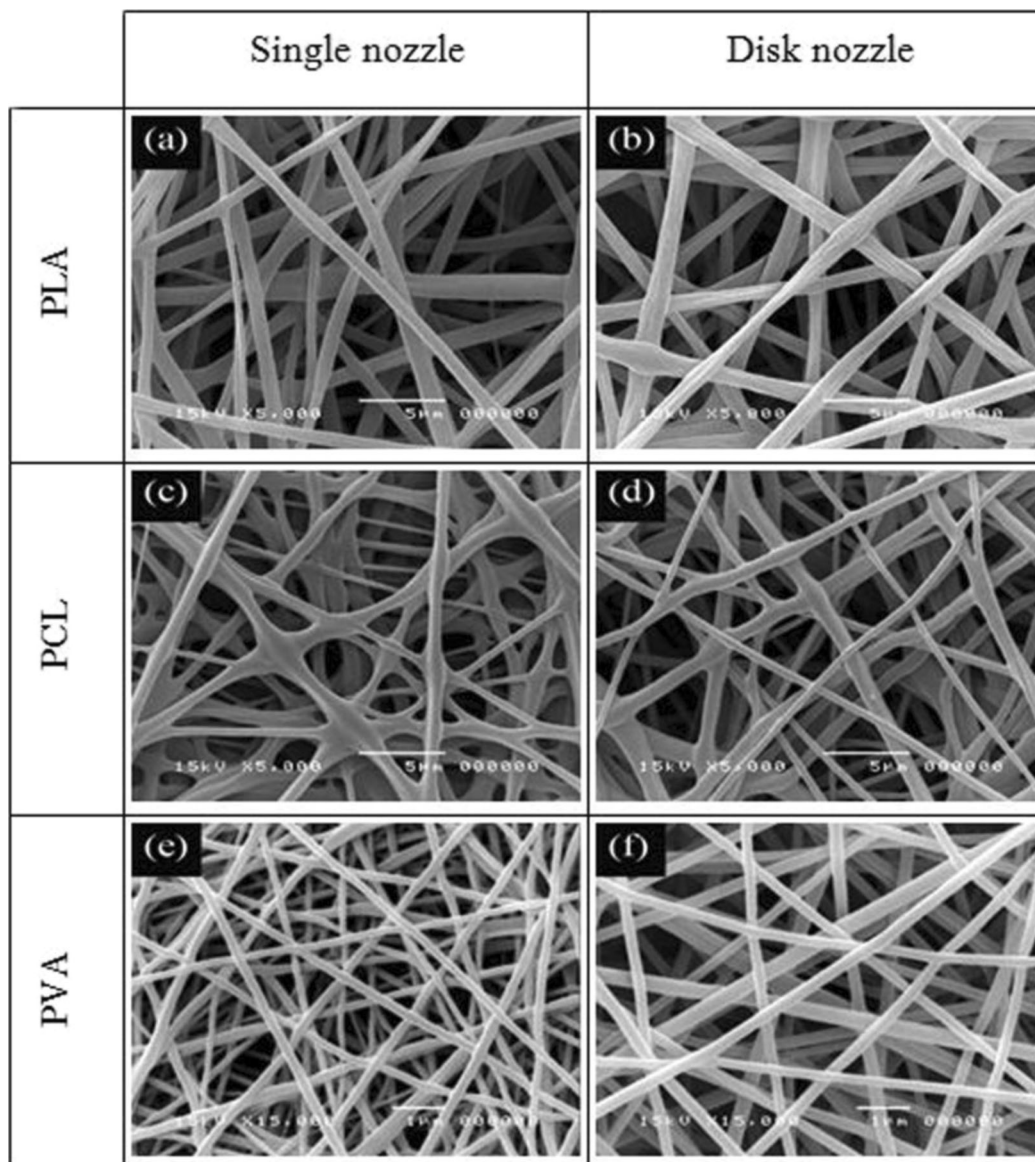

electrospun nanofiber mats collected from both systems were similar and almost identical. As shown in Table 1, disk-spun PCL nanofibers in this study showed moderate fusing of the fibers, similar to the PCL nanofibers spun by the conventional single nozzle electrospinning method. On the other hand, disk-spun PLA and PVA nanofibers also demonstrated similar morphology as their conventionally spun counterparts but the disk-spun PLA fibers were slightly rougher on the surface.

Fiber size distribution

Disk-spun PLA nanofiber mats demonstrated a fiber size distribution curve similar to conventionally spun PLA nanofiber mats. As shown in Fig. 6, nanofibers obtained from rotating-disk electrospinning and the conventional single nozzle process fit between 500 nm to 1600 nm and 200 nm to 1400 nm respectively. Although rotating-disk electrospinning could achieve similar distribution to that of conventionally spun samples, there is a positive gain in distribution which means the average fiber diameter is slightly larger than conventionally spun PLA nanofibers at 935 nm compared to 741 nm. Looking at Fig. 6, we can see that the distribution curve is shifted to the right but with similar curve geometry as the conventional single nozzle electrospinning.
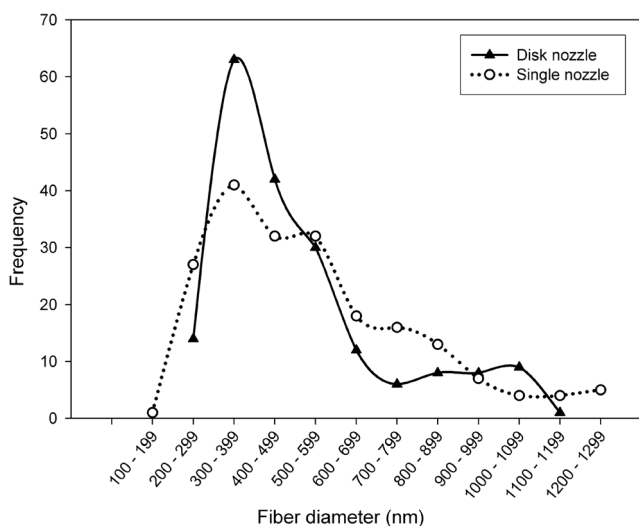
On the other hand, the fiber size distribution of disk-spun PCL nanofibers is narrower compared to the samples
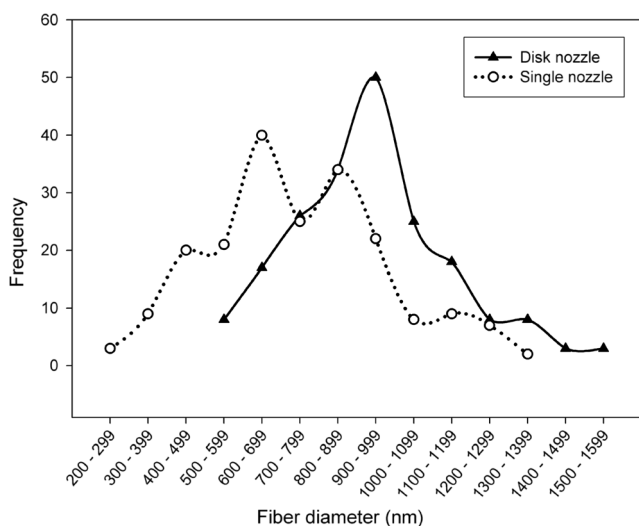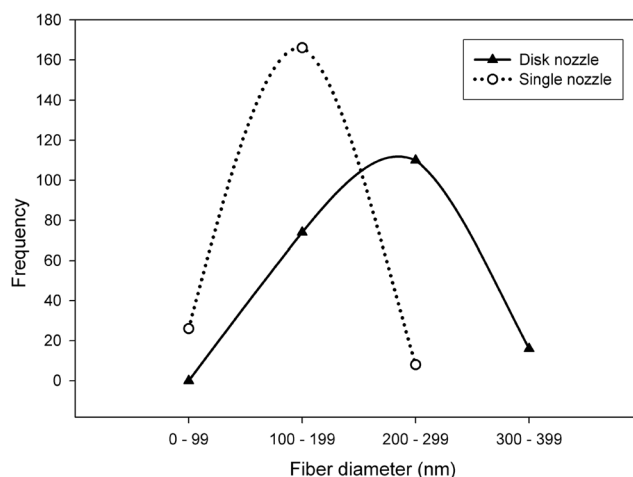
Fig. 6 Fiber size distribution of fiber diameter of 10% w/v PLA in DMF/DCM mixed solvent (ratio: 3:7)

Fig. 8 Fiber size distribution of fiber diameter of 12% w/v PVA aqueous solution

obtained by the conventional single nozzle electrospinning method, where the fiber diameters of disk-spun samples fit between 200 nm to 1200 nm but conventionally spun nanofibers start at 100 nm and go up to 1300 nm. From Fig. 7, we can clearly see that the fiber size distribution from the disk-spun samples is narrower and yielded nanofiber mats with average fiber diameters of 536 nm which is marginally smaller than 547 nm for conventionally spun nanofiber mats.

The fiber size distribution of disk-spun PVA nanofibers is broader than conventionally spun nanofibers but both fall into the range of less than 400 nm. As shown in Fig. 8, conventional single nozzle electrospinning is able to produce smaller fibers ranging between 63 nm to 300 nm with an average

diameter of 129 nm where the distribution for disk-spun fibers is broader with fiber diameters going up to 400 nm with an average diameter of 216 nm.

Taylor cone analysis

The main aim of this study is to develop an electrospinning system that could match or improve on the conventional single nozzle electrospinning technique. The fundamental basis of the electrospinning process is the formation of the Taylor Cone and jetting of polymer solution once the threshold voltage is reached [41], while Yarin et al. reported that a polymeric Taylor Cone has a half angle (α) ranging between 32° to 46°. Measurements done by imaging software have confirmed that the Taylor Cone in this system had a half angle of 38.7° and it is illustrated in Fig. 9.

Fig. 7 Fiber size distribution of fiber diameter of 12% w/v PCL in DMF/DCM mixed solvent (ratio: 1:1)
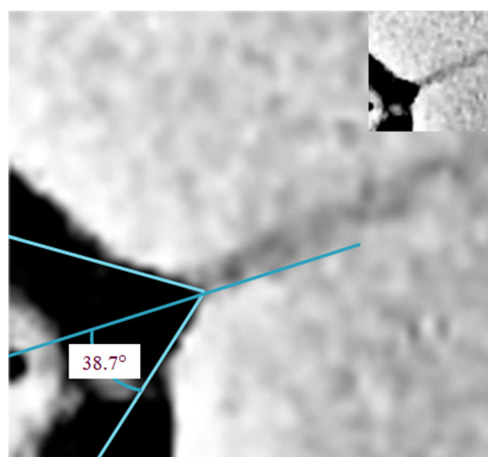
Fig. 9 Half angle (α) measurement of Taylor cone from disk electrospinning system

Conclusion

Rotating-disk electrospinning has demonstrated a much higher productivity level compared to its predecessor. Moreover, nanofiber mats produced by this process are comparable to those from the conventional single nozzle electrospinning technique in terms of morphology and fiber size distribution. This new process can be easily operated and there is no clogging compared to the conventional set-up. Nonetheless, rotating-disk electrospinning can be used with different polymers of different solvent systems. In this work, we have also demonstrated that polymeric nanofibers could be electrospun at relatively low voltages compared to conventional electrospinning in spite of the extra forces that have to be overcome.

References

1. Van de Witte P, Dijkstra PJ, Van den Berg JWA, Feijen J (1996) Phase separation processes in polymer solutions in relation to membrane formation. J Membr Sci 117:1–31

2. Chakarvarti SK, Vetter J (1998) Template synthesis—a membrane based technology for generation of nano−/micro materials: a review. Radiat Meas 29:149–159

3. Long Y-Z, Li M-M, Gu C, Wan M, Duvail J-L, Liu Z, Fan Z (2011) Recent advances in synthesis, physical properties and applications of conducting polymer nanotubes and nanofibers. Prog Polym Sci 36:1415–1442

4. Shuguang Z (2002) Emerging biological materials through molecular self-assembly. Biotechnol Adv 20:321–339

5. Perez, M., Swan, M., Louks, J., 2000. US Patent 6,110,588

6. Pourdeyhimi, B., Fedorova, N., Sharp, S., 2006. U.S. Patent 2006292355

7. Merkulov VI, Melechko AV, Guillorn MA, Simpson ML, Lowndes DH, Whealton JH, Raridon RJ (2002) Controlled alignment of carbon nanofibers in a large-scale synthesis process. Appl Phys Lett 80:4816–4818

8. Xie J, Li X, Xia Y (2008) Putting electrospun nanofibers to work for biomedical research. Macromol Rapid Commun 29:1775–1792

9. Supaphol P, Suwantong O, Sangsanoh P and Neamnark A (2001) In: Reisner DE (ed) Bionanotechnology II: Global Prospects, CRC Press, Boca Raton

10. Cui W, Zhou Y, Chang J (2010) Electrospun nanofibrous materials for tissue engineering and drug delivery. Sci Technol Adv Mater 11:014108

11. Zahedi P, Rezaeian I, Ranaei-Siadat S-O, Jafari S-H, Supaphol P (2010) A review on wound dressings with an emphasis on electrospun nanofibrous polymeric bandages. Polym Adv Technol 21:77–95

12. Qin X-H, Wang S-Y (2006) Filtration properties of electrospinning nanofibers. J Appl Polym Sci 102:1285–1290

13. Wang X, Hsiao BS (2016) Electrospun nanofiber membranes. Curr Opin Chem Eng 12:62–81

14. Agarwal S, Greiner A, Wendorff JH (2013) Functional materials by electrospinning of polymers. Prog Polym Sci 38:963–991

15. Teo W-E, Inai R, Ramakrishna S (2011) Technological advances in electrospinning of nanofibers. Sci Technol Adv Mater 12:013002

16. Zhou F-L, Gong R-H, Porat I (2009) Mass production of nanofibre assemblies by electrostatic spinning. Polym Int 58:331–342

17. Nayak R, Padhye R, Kyratzis IL, Truong YB, Arnold L (2012) Recent advances in nanofibre fabrication techniques. Text Res J 82:129–147

18. Kumar A, Wei M, Barry C, Chen J, Mead J (2010) Controlling fiber repulsion in multijet electrospinning for higher throughput. Macromol Mater Eng 295:701–708

19. Srivastava Y, Marquez M, Thorsen T (2007) Multijet electrospinning of conducting nanofibers from microfluidic manifolds. J Appl Polym Sci 106:3171–3178

20. Varesano A, Carletto RA, Mazzuchetti G (2009) Experimental investigations on the multi-jet electrospinning process. J Mater Process Technol 209:5178–5185

21. Deng W, Gomez A (2007) Influence of space charge on the scale-up of multiplexed electrosprays. J Aerosol Sci 38:1062–1078

22. Ding B, Kimura E, Sato T, Fujita S, Shiratori S (2004) Fabrication of blend biodegradable nanofibrous nonwoven mats via multi-jet electrospinning. Polymer 45:1895–1902

23. Theron SA, Yarin AL, Zussman E, Kroll E (2005) Multiple jets in electrospinning: experiment and modeling. Polymer 46:2889–2899

24. Xie S, Zeng Y (2012) Effects of electric field on multineedle electrospinning: experiment and simulation study. Ind Eng Chem Res 51:5336–5345

25. Zhou F-L, Gong R-H, Porat I (2010) Needle and needleless electrospinning for nanofibers. J Appl Polym Sci 115:2591–2598

26. Huang Z-M, Zhang YZ, Kotaki M, Ramakrishna S (2003) A review on polymer nanofibers by electrospinning and their applications in nanocomposites. Compos Sci Technol 63:2223–2253

27. Yarin AL, Zussman E (2004) Upward needleless electrospinning of multiple nanofibers. Polymer 45:2977–2980

28. Niu H, Wang X, Lin T (2011) Needleless electrospinning: influences of fibre generator geometry. J Text Inst 2011:1–8

29. Kostakova E, Meszaros L, Gregr J (2009) Composite nanofibers produced by modified needleless electrospinning. Mater Lett 63:2419–2422

30. Niu H, Lin T, Wang X (2009) Needleless electrospinning. I. A comparison of cylinder and disk nozzles. J Appl Polym Sci 114:3524–3530

31. Niu H, Lin T (2012) Fiber generators in needleless electrospinning. J Nanomater 2012:1–13

32. Wang X, Niu H, Wang X, Lin T (2012) Needleless electrospinning of uniform nanofibers using spiral coil spinnerets. J Nanomater 2012:1–9

33. Forward KM, Rutledge GC (2012) Free surface electrospinning from a wire electrode. Chem Eng J 183:492–503

34. Brettmann BK, Tsang S, Forward KM, Rutledge GC, Myerson AS, Trout BL (2012) Free surface electrospinning of fibers containing microparticles. Langmuir 28:9714–9721

35. Dosunmu OO, Chase GG, Kataphinan W, Reneker DH (2006) Electrospinning of polymer nanofibres from multiple jets on a porous tubular surface. Nanotechnology 17:1123–1127

36. Varabhas JS, Chase GG, Reneker DH (2008) Electrospun nanofibers from a porous hollow tube. Polymer 49:4226–4229

37. Fuh Y-K, Lien L-C, Chen S-Y (2012) High-throughput production of nanofibrous mats via a porous materials electrospinning process. J Macromol Sci, Part B 51:1742–1749

38. He J-H, Liu Y, Xu L, Yu J-Y, Sun G (2008) BioMimic fabrication of electrospun nanofibers with high-throughput. Chaos, Solitons Fractals 37:643–651

39. Liu Y, Dong L, Fan J, Wang R, Yu J-Y (2011) Effect of applied voltage on diameter and morphology of ultrafine fibers in bubble electrospinning. J Appl Polym Sci 120:592–598

40. Yang R, He J, Xu L, Yu J (2009) Bubble-electrospinning for fabricating nanofibers. Polymer 50:5846–5850

41. Yarin AL, Koombhongse S, Reneker DH (2001) Taylor cone and jetting from liquid droplets in electrospinning of nanofibers. J Appl Phys 90:4836–4846